Journal of Biomedical Optics

SPIEDigitalLibrary.org/jbo

Endoscopic swept-source optical coherence tomography based on a two-axis microelectromechanical system mirror

Donglin Wang
Linlai Fu
Xin Wang
Zhongjian Gong
Sean Samuelson
Can Duan
Hongzhi Jia
Jun Shan Ma
Huikai Xie

SPIE

Endoscopic swept-source optical coherence tomography based on a two-axis microelectromechanical system mirror

Donglin Wang,[a,b] Linlai Fu,[b] Xin Wang,[c] Zhongjian Gong,[c] Sean Samuelson,[d] Can Duan,[d] Hongzhi Jia,[a] Jun Shan Ma,[a] and Huikai Xie[d]

[a]University of Shanghai for Science and Technology, Ministry of Education, Shanghai Key Lab of Modern Optical System, Engineering Research Center of Optical Instrument and System, No. 516 JunGong Road, Shanghai 200093, China
[b]WiO Technology Ltd., Co., Wuxi, Jiangsu 214028, China
[c]Wuxi People's Hospital of Nanjing Medical University, No. 299, Qingyang Road, Wuxi 214023 Jiangsu, China
[d]University of Florida, Department of Electrical and Computer Engineering, Gainesville 32611, Florida

Abstract. A microelectromechanical system (MEMS) mirror based endoscopic swept-source optical coherence tomography (SS-OCT) system that can perform three-dimensional (3-D) imaging at high speed is reported. The key component enabling 3-D endoscopic imaging is a two-axis MEMS scanning mirror which has a 0.8×0.8 mm^2 mirror plate and a 1.6×1.4 mm^2 device footprint. The diameter of the endoscopic probe is only 3.5 mm. The imaging rate of the SS-OCT system is 50 frames/s. OCT images of both human suspicious oral leukoplakia tissue and normal buccal mucosa were taken *in vivo* and compared. The OCT imaging result agrees well with the histopathological analysis. © *2013 Society of Photo-Optical Instrumentation Engineers (SPIE)* [DOI: 10.1117/1.JBO.18.8.086005]

Keywords: optical coherence tomography; microelectromechanical system mirror; oral cancer.

Paper 130091RR received Feb. 17, 2013; revised manuscript received Jul. 4, 2013; accepted for publication Jul. 9, 2013; published online Aug. 12, 2013.

1 Introduction

Optical coherence tomography (OCT) has become a powerful medical imaging modality due to its noninvasive, high-resolution, real-time cross-sectional imaging capability[1] and has been widely applied clinically in ophthalmology, dermatology, and cardiology.[2–4] A large effort has also been made to develop endoscopic OCT for applications in human internal organs,[5,6] but it is hindered by the stringent size requirements for use inside the human body. Microelectromechanical system (MEMS) is an emerging technology that has the advantages of small size, fast speed, and low cost. MEMS-based OCT has been studied for over a decade. For example, Pan et al. reported the first MEMS-based OCT in 2001.[7] Since then, MEMS-OCT has been demonstrated by using MEMS mirrors based on electrostatic,[8] electrothermal,[9] electromagnetic,[10] and piezoelectric[11] actuation. Most of these MEMS-OCT systems employed time-domain OCT,[12–14] and others used spectral-domain OCT.[15,16] Endoscopic swept source (SS) OCT has also been demonstrated by using a rotating micromotor,[17] a resonant piezotube scanner,[18] or two resonating MEMS lens scanners.[19] Rotating micromotors can only perform side-view imaging, and resonant scanners utilizing Lissajous patterns complicate data acquisition and image processing.

In this article, we report a MEMS mirror-based endoscopic SS-OCT. The MEMS mirror scans along both x-axis and y-axis with a linear raster pattern. Three-dimensional (3-D) images can be acquired without the need of any external motors or resonant scan. A high speed of 50 frames/s OCT image rate is achieved. In contrast, our previous MEMS OCT system was based on a time-domain OCT system with low imaging rate of 2.5 frames/s.[13] In addition to the employment of a sweep source, the MEMS probe design of our new endoscopic SS-OCT system has been much improved. First, the MEMS holder and the alignment trenches are redesigned for more reliable assembling and better alignment accuracy. Second, a much more robust stainless steel tube is used to replace the plastic tube. Third, a flat glass optical window is designed to reduce the astigmatism present in our previous plastic tube–based probes. Furthermore, the MEMS driving signal is fine tuned to guarantee linear raster scan. With these efforts, a clinical experiment has been successfully performed.

2 Materials and Methods

Figure 1 shows a 3-D model and a picture of the endoscopic probe. The outer diameter and length of the probe are 3.5 and 15 mm, respectively. It is composed of a mount base, a gradient reflective index (GRIN) lens with a diameter of 1 mm, a single-mode fiber aligned and assembled with the GRIN lens in a glass sleeve, and a MEMS mirror shown in Fig. 1(c). The MEMS mirror is based on electrothermal actuation and has four pairs of unique dual S-shaped bimorph structures to achieve large dual-axis scan range at low drive voltage, which is similar to the one reported in Ref. 20. The active mirror plate is 0.8×0.8 mm^2 and the chip size is 1.6×1.4 mm^2. The MEMS mirror is flip chip bonded on a flexible printed circuit board (FPCB) that provides electrical connection and mechanical support to the MEMS mirror.

Address all correspondence to: Zhongjian Gong, Wuxi People's Hospital of Nanjing Medical University, No. 299, Qingyang Road, Wuxi 214023, Jiangsu, China. Tel: 86-13358112050; Fax: 86-510-82700778; E-mail: gongzj@wuxiph.com, or Hongzhi Jia, University of Shanghai for Science and Technology, Ministry of Education, Shanghai Key Lab of Modern Optical System, Engineering Research Center of Optical Instrument and System, No. 516 JunGong Road, Shanghai 200093, China. Tel: 86-21-55782523; Fax: 86-21-55271419; E-mail: hzjia@usst.edu.cn

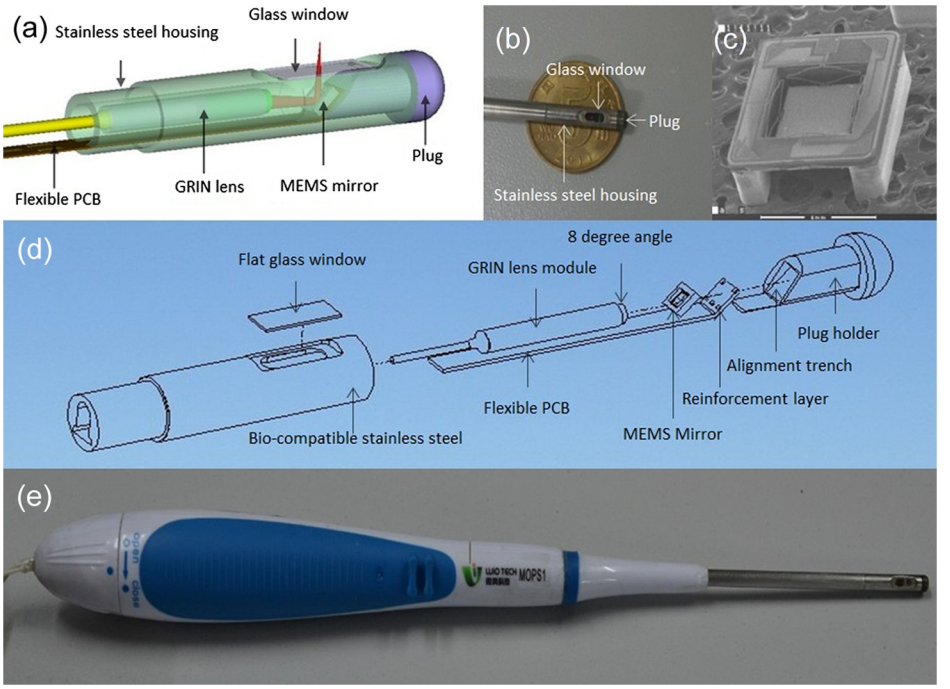

Fig. 1 (a) Three-dimensional (3-D) model of the MEMS-based endoscopic probe; (b) a photo of an assembled probe; (c) dual S-shape bimorph MEMS mirror; (d) exploded view of the probe assembly; and (e) the complete handheld OCT probe (210 mm long).

Figure 1(d) shows the exploded view of the probe assembly. The MEMS mirror can be easily aligned with the GRIN lens by the trench in the plug holder. A number of major improvements have been made, compared to prior probe designs,[13,20,21] to enhance the robustness and applicability at clinical settings. First, the fiber and GRIN lens are packaged into a single module and the GRIN lens is cut with 8 deg at both ends to minimize back reflection and thus greatly reduce artifacts. Second, a reinforcement layer is added in the FPCB bonding area to increase its surface flatness and thus ensures a more reliable bonding for the MEMS mirror. This is critical for long-term use. Third, the probe consists of a separate plug holder which can be easily assembled with the main body of the probe. So the MEMS mirror can be placed and fixed on the plug holder outside the probe, which greatly simplifies the procedure and improves the reliability of the MEMS mirror packaging. Fourth, the probe body is made of biocompatible stainless steel to provide high robustness and effective heat conduction. The temperature at the surface of a working probe is no more than >3°C above the ambient temperature which ensures the safe use of this endoscope probe in human body. Last, a glass window is used to seal the probe cavity and allows the light to pass through. It has been shown that a flat optical window leads to much smaller light spot distortion and significantly reduced astigmatism, compared to a cylindrical tube which inevitably stretches the light spot in the transverse direction of the tube.[21] The assembly process of the probe becomes more accurate and reliable with the above significant improvements.

For safe use of the probe, electrical hazard prevention is also taken into account in the probe design. The MEMS mirror in the probe operates at a low voltage with a maximum value of 4.5 V, which is safe for the human body. Specifically, the maximum current in the electrical lines is limited to <23 mA with an external resistor. The MEMS chip is bonded on a FPCB whose conductive wires are all wrapped by nonconductive materials. The electrical wires inside the stainless steel tube and the extension cable are all coated with an insulating plastic. Last, the optical power incident on the tissue is about 1 mW which is a safe exposure level according to ANSI Z136 standards.[22]

The schematic of the whole system is shown in Fig. 2, which includes the MEMS mirror-based endoscopic probe and an SS-OCT system. The SS laser (Axsun Tech., Billerica, Massachusetts) has a center wavelength of 1310 nm and a FWHM bandwidth of about 80 nm. The laser sweeps in *k*-space at 50 kHz and generates a linear K clock sequence for axial scan (A-scan). The maximum number of K clocks in each sweeping period is 1286. In our experiment, we select 1024 K points for each A-scan, which are converted to 512 depth points. The MEMS mirror generates a fast-axis scan and a slow-axis scan. The voltage signals applied are with triangular waveforms

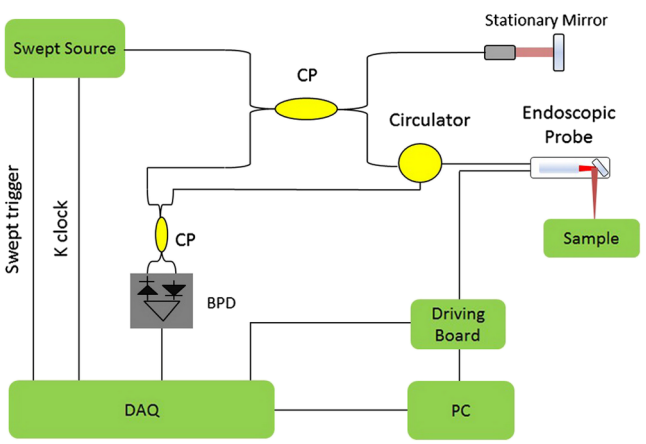

Fig. 2 MEMS-based endoscopic SS-OCT system. CP: 2 × 2 fiber coupler; BPD: balanced photo detector; Control Board: output scan driving signal to probe and sync signal to DAQ board for data acquiring.

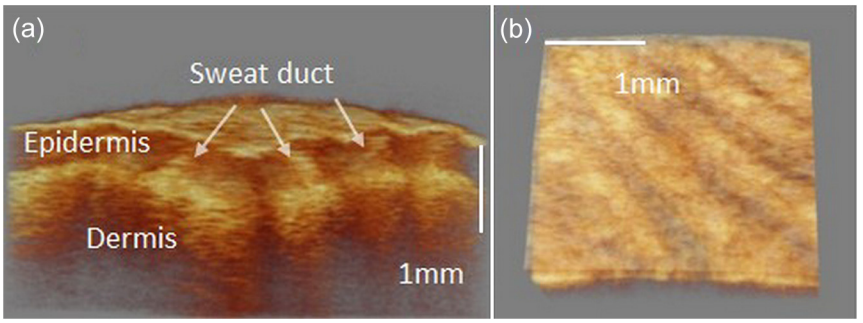

Fig. 3 *In vivo* image of a human fingertip. (a): front view of 3-D image and (b) enface image.

varying from 0 to 4 V, which correspond to the linear angular scan range of the MEMS mirror. The fast axis scans 28 deg at 50 Hz and 512 sample points are taken. So each cross-sectional image, or an image frame, has 512×512 pixels. The OCT images are displayed real time on a screen at 50 frames/s. The slow axis scans 28 deg at 450 mHz, and the images are stored and reconstructed to form 3-D images. Both the fast-axis and slow-axis scan signals are triangular waves generated by a data acquisition card (NI PCI6722). The signals are smoothened by adding a low-pass filter, respectively, to reduce the ringing of the mirror plate at the turning points of the triangular waveforms. The residual ringing will still cause image blurring of several pixels at both the beginning and the end of each OCT image frame. The NI card also outputs a synchronization signal for each frame acquisition. A high speed data acquisition board (Alazartech Tech., ATS9350) is employed to receive the sweeping trigger, synchronize the acquisition signal, and sample the interference signal at the K clock timing.

3 Results and Discussion

Figure 3 shows imaging results of a human finger using this MEMS OCT system. As shown in Fig. 3(a), the top surface layer is stratum corneum, and the epidermis and sweat duct are also clearly visible. Figure 3(b) shows a top view of an area of 2×2 mm^2 fingerprint. The measured insertion loss of the probe is 0.5 dB. The sensitivity of the OCT system was measured by using a pigtailed fiber with a return loss of 66 dB. The signal to noise ratio of the recorded OCT signal with that pigtailed fiber is 32 dB. So the sensitivity of the OCT system is about 98 dB. The probe focal point is at 2.0 mm from the surface of the optical window, where the axial resolution is 10.6 μm which was measured in the air based on the point spread function. We also measured the lateral resolution by imaging a USAF-1951 card and the 17.5 μm lines were clearly identified, as shown in Fig. 4.

In order to further validate the practical use of this system, we conducted *in vivo* imaging experiments on a suspicious oral cancer of a human patient using our MEMS-based SS-OCT system. Oral cancer is the sixth most often occurring cancer in the world. Oral leukoplakia (OL) is visible as adherent white patches on the mucous membranes of the oral cavity and sometimes described as precancer. The clinical experiments were conducted in Wuxi No. 1 People's Hospital with a protocol approved by the hospital's research ethics board, and informed consent was obtained from the volunteer patient. A 65-year-old woman with no major medical conditions was present with a 2-month history of painless white ulcerated lesions in the middle of the buccal mucosa. The round ulcers were measured from 0.8 to 2.4 cm in diameter with clean, smooth bases and slightly elevated, indurated borders.

To compare the white ulcers with normal mucosa, a normal oral mucosa area was scanned using the OCT probe at the first. Before the probe was inserted into the patient orally, it was dipped in 75% alcohol >15 min for sterilization and cleaned by sterile cotton balls. When scanning the tissue, the probe was slightly pressed on the tissue surface to make sure it made contact with the probe glass window because the sample needs to remain stationary with respect to the probe during the scan time of about 2 s. After all the areas of interest were scanned, the probe was dipped into another 75% alcohol and disinfected. The probe can be reused after receiving pressure steam sterilization.

Figure 5 shows an OCT image of the normal buccal mucosa, which has three distinct layers: epithelium (EP) on the top,

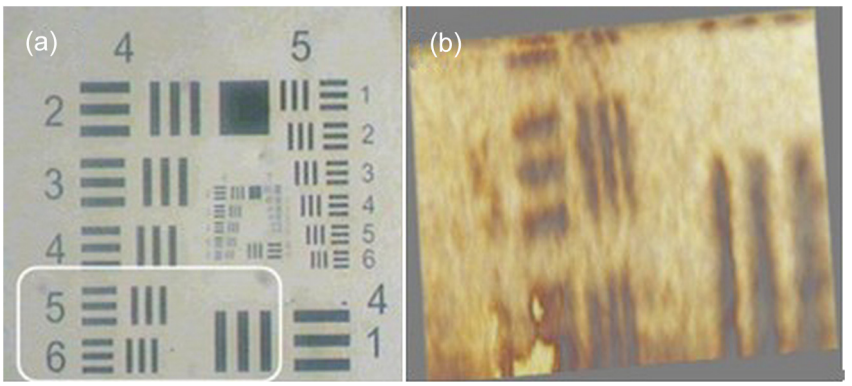

Fig. 4 Resolution test. Group 4 element 6 (a) can be identified in OCT image (b).

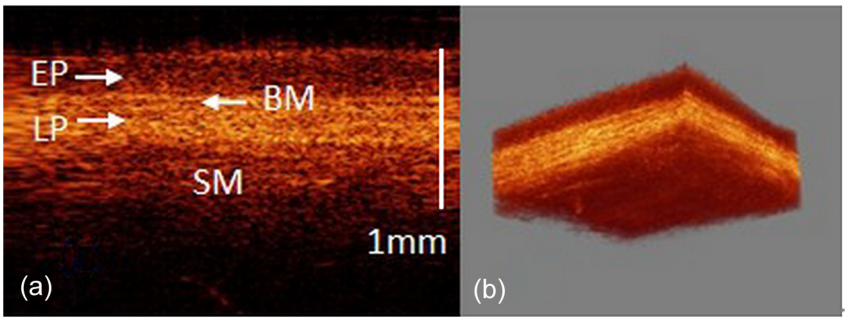

Fig. 5 OCT image of normal buccal mucosa. (a): two-dimensional (2-D) image and (b) 3-D image reconstruction.

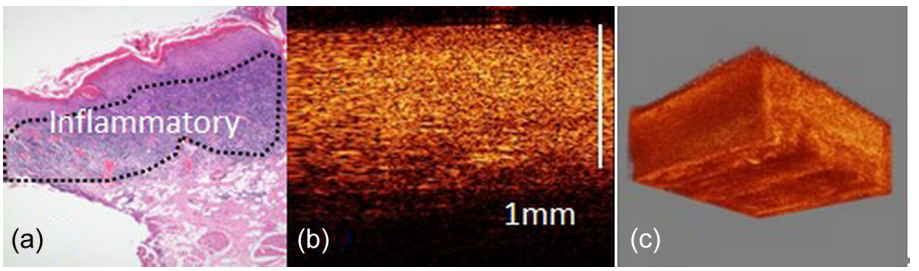

Fig. 6 Histopathological image of oral leukoplakia mucosa (a) shows inflammatory cells have infiltrated into nearby tissues. OCT images (b) and (c) also show that basement membrane (BM) is disappeared.

lamina propria (LP) in the middle, and submucosa (SM) at the bottom. Their boundaries can be clearly delineated, especially for the basement membrane (BM) between EP and LP. Then the probe was scanned over the white lesion area. Figure 6 shows an OCT image of a suspicious precancerous OL area. In this case, no clear layer structures can be identified. After imaging the OL region by OCT, a biopsy was taken. Histopathological images show that the BM boundary has disappeared and inflammatory cells have infiltrated into nearby tissues, which is in good agreement with the OCT imaging result. The patient was then clinically diagnosed as atypical hyperplasia with inflammation. At the follow-up check 6 months after the surgery, there were no signs of recurrence.

Although many MEMS-based time domain (TD)-OCT systems can also obtain 3-D volumetric imaging, they require a rapid scanning optical delay line (RSOD) to realize A-scan. The RSOD scan rate is typically of several kilohertz, which limits the imaging rate of TD-OCT to only a few frames/s. In contrast, this MEMS-based SS-OCT can achieve 50 kHz A-scan that can realize 50 frames/s for real-time imaging. On the other hand, the coherence length of the SS is relatively large in the range of 10 to 15 mm, so interference signals are generated in various interfaces in the system, e.g., the fiber ends, the GRIN lens end surfaces, the MEMS mirror surface, and both surfaces of the glass window. These interfaces must be carefully designed or processed; otherwise they may introduce many artifacts into OCT images.

4 Conclusion

In summary, we have developed a MEMS-based endoscopic SS-OCT system and performed *in vivo* diagnosis of oral dysplasia. The imaging speed is 50 frames/s and imaging depth inside the oral mucosa is about 1.5 mm. The *in vivo* OCT images successfully delineated the tissue structure of normal mucosa and revealed the disappearance of the base membrane layer in the dysplasia area. The probe is designed for easy assembly and low cost at the expense of a larger diameter. There is a trade-off between the probe diameter and cost. Although the probe is 0.7 mm larger in diameter than the previous one, it fits well in oral applications. The same robust probe design can be further reduced in diameter and thus has the potential for other clinical uses including the airways or gastrointestinal tracts. The current probe works at a side-view mode and a forward-looking type will be developed to expand the application areas.

Acknowledgments

This work is supported in part by the Innovation Fund Project for Graduate Student of Shanghai (JWCXSL1201) and the US National Science Foundation under award#1002209.

References

1. D. Huang et al., "Optical coherence tomography," *Science* **254**(5035), 1178–1181 (1991).
2. J. S. Schuman et al., "Optical coherence tomography: a new tool for glaucoma diagnosis," *Curr. Opin. Ophthalmol.* **6**(2), 89–95 (1995).
3. J. Welzel, "Optical coherence tomography in dermatology: a review," *Skin Res. Technol.* **7**(1), 1–9 (2001).
4. S.H. Yun et al., "Comprehensive volumetric optical microscopy in vivo," *Nat. Med.* **12**(12), 1429–1433 (2006).
5. G. J. Tearney et al., "In vivo endoscopic optical biopsy with optical coherence tomography," *Science* **276**(5321), 2037–2039 (1997).
6. M. V. Sivak, Jr. et al., "High-resolution endoscopic imaging of the GI tract using optical coherence tomography," *Gastrointest. Endosc.* **51**(4), 474–479 (2000).
7. Y. Pan, H. Xie, and G. K. Fedder, "Endoscopic optical coherence tomography based on a microelectromechanical mirror," *Opt. Lett.* **26**(24), 1966–1968 (2001).
8. J. M. Zara et al., "Electrostatic micromachine scanning mirror for optical coherence tomography," *Opt. Lett.* **28**(8), 628–630 (2003).

9. T. Xie et al., "Endoscopic optical coherence tomography with a modified microelectromechanical systems mirror for detection of bladder cancers," *Appl. Opt.* **42**(31), 6422–6426 (2003).
10. K. H. Kim et al., "Two-axis magnetically-driven MEMS scanning catheter for endoscopic high-speed optical coherence tomography," *Opt. Express* **15**(26), 18130–18140 (2007).
11. F. Filhol et al., "Resonant micro-mirror excited by a thin-film piezoelectric actuator for fast optical beam scanning," *Sens. Actuat. A* **123**, 483–489 (2005).
12. W. Jung et al., "Three-dimensional endoscopic optical coherence tomography by use of a two-axis microelectromechanical scanning mirror," *Appl. Phys. Lett.* **88**(16), 163901 (2006).
13. J. Sun et al., "3D in vivo optical coherence tomography based on a low-voltage, large-scan-range 2D MEMS mirror," *Opt. Express* **18**(12), 12065–12075 (2010).
14. Y. Xu et al., "Design and development of a 3D scanning MEMS OCT probe using a novel SiOB package assembly," *J. Micromech. Microeng.* **18**(12), 125005 (2008).
15. A. D. Aguirre et al., "Two-axis MEMS scanning catheter for ultrahigh resolution three-dimensional and En Face imaging," *Opt. Express* **15**(5), 2445–2453 (2007).
16. J. M. Zara and P. E. Patterson, "Polyimide amplified piezoelectric scanning mirror for spectral domain optical coherence tomography," *Appl. Phys. Lett.* **89**(26), 263901 (2006).
17. J. Su et al., "In vivo three-dimensional microelectromechanical endoscopic swept source optical coherence tomography," *Opt. Express* **15**(16), 10390–10396 (2007).
18. S. Moon et al., "Semi-resonant operation of a fiber-cantilever piezotube scanner for stable optical coherence tomography endoscope imaging," *Opt. Express* **18**(20), 21183–21197 (2010).
19. H.C. Park et al., "Forward imaging OCT endoscopic catheter based on MEMS lens scanning," *Opt. Lett.* **37**(13), 2673–2675 (2012).
20. S. Samuelson et al., "A 2.8-mm imaging probe based on a high-fill-factor mems mirror and wire-bonding-free packaging for endoscopic optical coherence tomography," *J. Microelectromech. Syst.* **21**, 1291–1302 (2012).
21. D. L. Wang et al., "Design optimization and implementation of a miniature optical coherence tomography probe based on a MEMS mirror," *Proc. SPIE* **8191**, 81910M (2011).
22. American National Standards Institute, *American National Standard for the Safe Use of Lasers: ANSI Z136.1-2000*, Laser Institute of America, Orlando, FL (2000).